

# HARDENING AND NON-ASSOCIATED FLOW NURBS PLASTICITY

WILLIAM M. COOMBS\*

\* School of Engineering & Computing Sciences,  
Durham University,  
Lower Mountjoy, South Road, Durham, DH1 3LE, UK.  
e-mail: w.m.coombs@dur.ac.uk, web page: www.dur.ac.uk

**Key words:** Computational plasticity, NURBS, non-associated flow, stress integration

**Abstract.** In numerical analysis the failure of engineering materials is controlled through specifying yield envelopes (or surfaces) that bound the allowable stress in the material. Simple examples include the prismatic von Mises (circle) and Tresca (hexagon) yield surfaces. However, each surface is distinct and requires a specific equation describing the shape of the surface to be formulated in each case. These equations impact on the numerical implementation (specifically relating to stress integration) of the models and therefore a separate algorithm must be constructed for each model. Recently a framework was proposed that allows any isotropic yield surface to be represented by a NURBS surface and the constitutive model formulated using the name numerical algorithm.

This paper presents, for the first time, an extension to this framework to allow both hardening (expansion/contraction of the surfaces) and a non-associated plastic flow rule. As with previous work on NURBS plasticity, the constitutive framework is combined with an implicit backward-Euler-type stress integration algorithm. The numerical performance of the algorithm is demonstrated using both material point investigations and boundary value simulations.

## 1 INTRODUCTION

Robust and efficient constitutive models are at the heart of every boundary value stress analysis problem, providing the essential link between stress and strain for the material that they represent. Elasto-plasticity is one class of inelastic material behaviour that allows these models to predict yield and capture post-yield behaviour. Central to these models is the concept of a yield surface that provides the boundary between elastic (inside the surface) and elasto-plastic behaviour (on the surface). However, such models are typically developed in rate form, providing a rate relationship between stress and strain that conflicts with an incremental boundary value solver, such as the finite element method. These boundary value solvers work with finite steps of stress and strain and therefore the rate-form constitutive relationships must be integrated. Typically the form of the yield

surface impacts on the stress integration algorithm with specific details change within the numerics (and code) for each implemented yield surface. This issue was overcome by the paper of Coombs et al. [1] for yield surfaces that are fixed in stress space, known as perfect plasticity. It allowed any smooth isotropic yield surface to be modelled without changing the numerical algorithm or underlying code by using non-uniform rational basis spline (NURBS) surfaces to represent the yield envelope. This paper extends that work to allow for isotropic expansion/contraction of the yield surface and for the evolution of plastic strains to be decoupled from the normal to the yield surface (that is, allowing a non-associated flow rule).

Here we follow the approach of Coombs et al. [1] and adopt an implicit stress integration algorithm coupled with a plasticity formulation that expresses the yield envelope as a NURBS surface. The key extensions that we allow here are for: (i) the yield surface to expand (hardening) or contract (softening) under plastic straining and (ii) decoupling the flow direction from the spatial gradient of the surface. This is achieved by allowing the position of the control points to be a function of inelastic straining and for the flow direction to be approximated by a separate NURBS basis. This extends the NURBS plasticity framework to include materials where the yield stress is a function of the history of plastic straining that the body has experienced and to those materials where an associated flow rule is not appropriate (such as geotechnical materials where an associated flow rule overestimates the volumetric dilation).

The layout of the paper is as follows, Section 2 provides the theoretical framework for hardening non-associated flow NURBS-based plasticity. Section 3 briefly explains the numerical implementation of the model and Section 4 provides some numerical examples. Finally, conclusions are drawn in Section 5.

## 2 NURBS PLASTICITY

This section provides the essential equations required to define an isotropically hardening NURBS surface and include it within a non-associated flow plasticity framework. For more detailed information on the construction of NURBS-based surfaces see the work of Piegler and Wayne [7] and the paper of Coombs et al. [1] for the particular case of perfect plasticity yield envelopes.

A general NURBS surface can be expressed in Haigh-Westergaard (H-W) coordinates as

$$S_k(\eta, \zeta) = \frac{\xi}{\sqrt{3}} \begin{Bmatrix} 1 \\ 1 \\ 1 \end{Bmatrix} + \sqrt{\frac{2}{3}}\rho \begin{Bmatrix} \sin(\theta + 2\pi/3) \\ \sin(\theta) \\ \sin(\theta - 2\pi/3) \end{Bmatrix}, \quad (1)$$

where the hydrostatic position  $\xi$ , radial coordinate  $\rho$  and Lode angle  $\theta$  are dependent on the values at the control points and the local position on the NURBS surface,  $\eta$  and  $\zeta$

$$\xi(\eta, \zeta) = \sum_{i=0}^n \sum_{j=0}^m R_{i,j}(\eta, \zeta) \Xi_{i,j}, \quad \rho(\eta, \zeta) = \sum_{i=0}^n \sum_{j=0}^m R_{i,j}(\eta, \zeta) P_{i,j} \quad (2)$$

and

$$\theta(\eta, \zeta) = \sum_{i=0}^n \sum_{j=0}^m R_{i,j}(\eta, \zeta) \Theta_{i,j}. \quad (3)$$

$\Xi_{i,j}$ ,  $P_{i,j}$  and  $\Theta_{i,j}$  are the control point values of the Haigh-Westergaard coordinates. The NURBS basis functions are given by

$$R_{i,j}(\xi, \eta) = \frac{N_{i,p}(\xi) N_{j,q}(\eta) w_{i,j}}{\sum_{k=0}^n \sum_{l=0}^m N_{k,p}(\xi) N_{l,q}(\eta) w_{k,l}}. \quad (4)$$

$N_{i,p}$  and  $N_{j,q}$  are the  $p^{\text{th}}$  and  $q^{\text{th}}$ -degree B-spline basis functions (see [2, 7], amongst others),  $\eta$  and  $\zeta$  are the local positions within the two Knot vectors that describe the surface and  $w_{i,j}$  are the weights associated with the control points. In the work of [1] the control points were defined in Cartesian coordinates, however in this paper we change to using H-W coordinates to allow for the extension to non-associated flow.

## 2.1 NURBS-based yield envelopes

Starting from the equation for a NURBS surface (1), a NURBS-based yield envelope [1] can be expressed as

$$f = \left( \sigma_i - S_i(\eta, \zeta, \varepsilon_i^{\text{P}}) \right) (S_{,\sigma})_i = 0, \quad (5)$$

where  $(S_{,\sigma})_i$  is the surface outward normal (that is, the partial derivative of  $S$  with respect to stress),  $\varepsilon_i^{\text{P}}$  is the principal plastic strain state and  $\sigma_i$  the principal stress state. The yield surface separates stress space into two regions: an elastic region where  $f < 0$  and an inadmissible region where  $f > 0$ . The boundary between these two regions ( $f = 0$ ) is used to define material failure and points on this surface will undergo elasto-plastic deformation. The outward normal to the yield envelope can be obtained through the cross product of the two local derivatives

$$(S_{,\sigma})_i = (S_{,\zeta} \times S_{,\eta})_i = \epsilon_{ijk} (S_{,\zeta})_j (S_{,\eta})_k, \quad (6)$$

where  $\epsilon_{ijk}$  is the Levi-Civita tensor<sup>1</sup>.  $S_{,\eta}$  and  $S_{,\zeta}$  are the derivatives of the NURBS surface with respect to the local coordinates  $\eta$  or  $\zeta$ .

## 2.2 Non-associated flow

In the case of non-associated flow the evolution of plastic strains is decoupled from the spatial gradient of the yield envelope. The plastic strains evolve according to

$$\dot{\varepsilon}_i^{\text{P}} = \dot{\gamma} (g_{,\sigma})_i, \quad (7)$$

---

<sup>1</sup> $\epsilon_{ijk} = 0$  if  $i = j$ ,  $j = k$  or  $k = i$ ,  $\epsilon_{ijk} = 1$  for even permutations of  $i$ ,  $j$  and  $k$  and  $\epsilon_{ijk} = -1$  for odd permutations of  $i$ ,  $j$  and  $k$ .

where  $\dot{\gamma}$  is the scalar plastic multiplier (or consistency parameter) and  $(g_{,\sigma})_i$  is the gradient of the plastic potential surface. This plastic multiplier must satisfy the Kuhn-Tucker-Karush consistency conditions

$$f(\sigma_i, \varepsilon_i^p) \leq 0, \quad \dot{\gamma} \geq 0 \quad \text{and} \quad f(\sigma_i, \varepsilon_i^p) \dot{\gamma} = 0. \quad (8)$$

These conditions enforce that the material must either be on the yield surface undergoing elasto-plastic deformation ( $f = 0$  and  $\dot{\gamma} \geq 0$ ) or inside the yield surface with purely elastic behaviour ( $f < 0$  and  $\dot{\gamma} = 0$ ).

In this NURBS plasticity approach the gradient of the plastic potential surface is given by

$$(g_{,\sigma})_i = \lambda_g \begin{Bmatrix} 1 \\ 1 \\ 1 \end{Bmatrix} + \sqrt{2} \begin{Bmatrix} \sin(\theta_g + 2\pi/3) \\ \sin(\theta_g) \\ \sin(\theta_g - 2\pi/3) \end{Bmatrix}, \quad (9)$$

where  $\lambda_g$  is the volumetric to deviatoric ratio of the plastic flow direction and  $\theta_g$  is the Lode angle of the plastic flow direction.  $\lambda_g$  and  $\theta_g$  are dependent on the corresponding control point values,  $\Lambda_{i,j}^g$  and  $\Theta_{i,j}^g$ , and the local position on the NURBS surface through

$$\lambda_g(\eta, \zeta) = \sum_{i=0}^n \sum_{j=0}^m R_{i,j}^g(\eta, \zeta) \Lambda_{i,j}^g \quad \text{and} \quad \theta_g(\eta, \zeta) = \sum_{i=0}^n \sum_{j=0}^m R_{i,j}^g(\eta, \zeta) \Theta_{i,j}^g. \quad (10)$$

The NURBS basis functions  $R_{i,j}^g(\eta, \zeta)$  are calculated in the same way as (4).

### 2.3 Isotropic hardening

Introducing hardening into the NURBS yield surfaces results in a yield surface that is dependent on the level of inelastic straining at a material point. This is included within the NURBS plasticity framework by allowing the control points to evolve with plastic straining, that is

$$\Xi = h(\varepsilon_i^p) \Xi^0 \quad \text{and} \quad P = h(\varepsilon_i^p) P^0 \quad (11)$$

where the superscript  $(\cdot)^0$  denotes the original control point coordinates and  $h(\varepsilon_i^p)$  controls the evolution of the control points. For linear isotropic hardening we can assume

$$h(\varepsilon_i^p) = 1 + \alpha \|\int_0^t \varepsilon_i^p dt\|, \quad (12)$$

where  $\alpha$  is a material constant controlling the hardening ( $\alpha > 0$ ) or softening ( $\alpha < 0$ ) rate and perfect plasticity is obtained with  $\alpha = 0$ . We can approximate the isotropic hardening function to provide an incremental function of the form

$$h(\Delta\varepsilon_i^p) = h_n + \alpha \|\Delta\varepsilon_i^p\|, \quad (13)$$

where  $h_n = h((\varepsilon_n^p)_i)$  is the value of the hardening function from the previously converged state and it is assumed that initially,  $h_0 = 1$ .

## 2.4 Stress integration

In this work we use an implicit elastic predictor, plastic corrector scheme [11], where the elastic trial stress is given by

$$\sigma_i^t = \sigma_i^n + \Delta\sigma_i, \quad \text{where} \quad \Delta\sigma_i = D_{ij}^e \Delta\varepsilon_j \quad \text{and} \quad \sigma_i^n = D_{ij}^e (\varepsilon_n^e)_j. \quad (14)$$

$(\varepsilon_n^e)_j$  and  $\sigma_i^n$  are the elastic strain and stress state from the previous load (or time) step in the global solution algorithm,  $\Delta\varepsilon_i$  is the strain increment associated with the global boundary value displacement and  $D_{ij}^e$  contains the principal components of the linear elastic stiffness matrix.

If the trial elastic stress state exceeds the yield envelope ( $f > 0$ ) then it must be corrected back onto the yield surface using a plastic stress increment, that is

$$\sigma_i^r = \sigma_i^t - \Delta\sigma_i^p, \quad \text{where} \quad \Delta\sigma_i^p = D_{ij}^e \Delta\varepsilon_j^p, \quad (15)$$

$\sigma_i^r$  is the *returned* stress state on the yield surface and  $\Delta\varepsilon_j^p$  is the plastic strain increment obtained from the incremental form of (7). Once this correction has been applied the updated elastic strain can be obtained from

$$(\varepsilon_{n+1}^e)_i = (\varepsilon_n^e)_i + \Delta\varepsilon_i - \Delta\varepsilon_i^p, \quad (16)$$

and the updated hardening parameter,  $h$ , from (13).

## 3 NUMERICAL IMPLEMENTATION

Consistent with the perfect plasticity implementation of Coombs et al. [1], here we use a coarse initial subdivision algorithm to provide the initial starting point for a backward Euler (bE) implicit stress integration process. This is to provide an initial estimate for the local positions within the Knot vectors,  $\eta$  and  $\zeta$  in (5) that act as the primary unknowns in the closest point projection (CPP) problem (in addition to the updated hardening parameter). However, despite this process being referred to as a CPP, the return stress is not generally the closest point geometrically in standard stress space.

In this paper we make use of energy-mapped space [3] to convert this CPP minimisation into a problem of finding the point on the yield envelope that the normal to the plastic potential surface passes through when intersecting with a trial point outside of the surface. Once the closest point solution in energy-mapped stress space has been found, the solution can be transformed back to conventional stress space. For a NURBS yield surface we only need to map the control point coordinates,  $(\Xi, P, \Theta)$ , and flow directions,  $(g, \sigma)_i$ , into energy-mapped space, the rest of the NURBS information remains unchanged.

As with the algorithm for associated flow perfect plasticity, the stress return path for bE procedure described in this paper starts and remains in the yield envelope and thereby satisfies the consistency conditions not only at the final state but also during the stress updating algorithm.

## 4 NUMERICAL ANALYSIS

This section presents both material point and boundary value simulations for the isotropically hardening/softening von Mises plasticity model represented and integrated in the NURBS plasticity framework. The yield surface can be expressed as

$$f = \rho - h\rho_y = 0, \quad (17)$$

where the deviatoric stress is  $\rho = \sqrt{2J_2}$  with  $J_2 = \frac{1}{2}s_{ij}s_{ji}$  and  $s_{ij} = \sigma_{ij} - \frac{1}{3}\sigma_{kk}\delta_{ij}$ ,  $\rho_y$  is the yield stress of the material and defines the radius of the von Mises cylinder.

### 4.1 Material point investigations

The stress integration errors for a von Mises yield surface with  $E = 200\text{Pa}$ ,  $\nu = 0.2$ ,  $\rho_y = 1\text{Pa}$  and  $\alpha = 10$  (hardening) using the NURBS integration procedure are shown in Figure 1. The stress state is initially located on the shear meridian in the  $\sigma_{zz} > \sigma_{yy} > \sigma_{xx}$  sextant of stress space. This point is then subjected to a stress increment that will take the trial stress state outside of the yield envelope into one of the three sextants shown in Figure 1. The space of trial states was explored for  $\rho_t/\rho_y \in [1, 6]$  and the errors associated with the trial state shown on the right of Figure 1. The normalised error measure used is

$$\text{error} = \frac{\|\{\sigma_{\text{NURBS}}\} - \{\sigma_e\}\|}{\|\sigma_e\|}, \quad (18)$$

where  $\{\sigma_{\text{NURBS}}\}$  is the stress return location associated with the NURBS model and  $\{\sigma_e\}$  is the exact stress return [5].

Although errors of over 20% are present in the model, exactly the same level of errors are observed in the von Mises yield surface integrated with a conventional bE stress integration procedure. As expected with any predictor-correction stress integration algorithm, the error increases as the tangential proportion of the stress increment increases. The errors are almost identical to those reported by Coombs et al. [1] for the perfect plasticity yield surface.

Figure 2 (i) shows the converged hardening parameter value for the same range of trial stress states as analysed in Figure 1. As expected, the value of the hardening parameter is only dependent on the magnitude of the plastic strain increment, or equivalently, the radial distance that the trial state is from the yield surface. Figure 2 (ii) gives the normalised error in the hardening parameter, the distribution of the error is similar to the stress errors shown in Figure 1 as the error in the stress increment will be proportional to the error in the return stress.

### 4.2 Plane strain double notched plate

Here we present the analysis of the plane strain stretching of a double-notched plate. The problem was initially presented by Nagtegaal *et al.* [6] for small strain plasticity to demonstrate the spurious response of standard finite-elements and was subsequently re-analysed in a number of papers, including [1, 4, 8, 9]. The plate had a Young's modulus

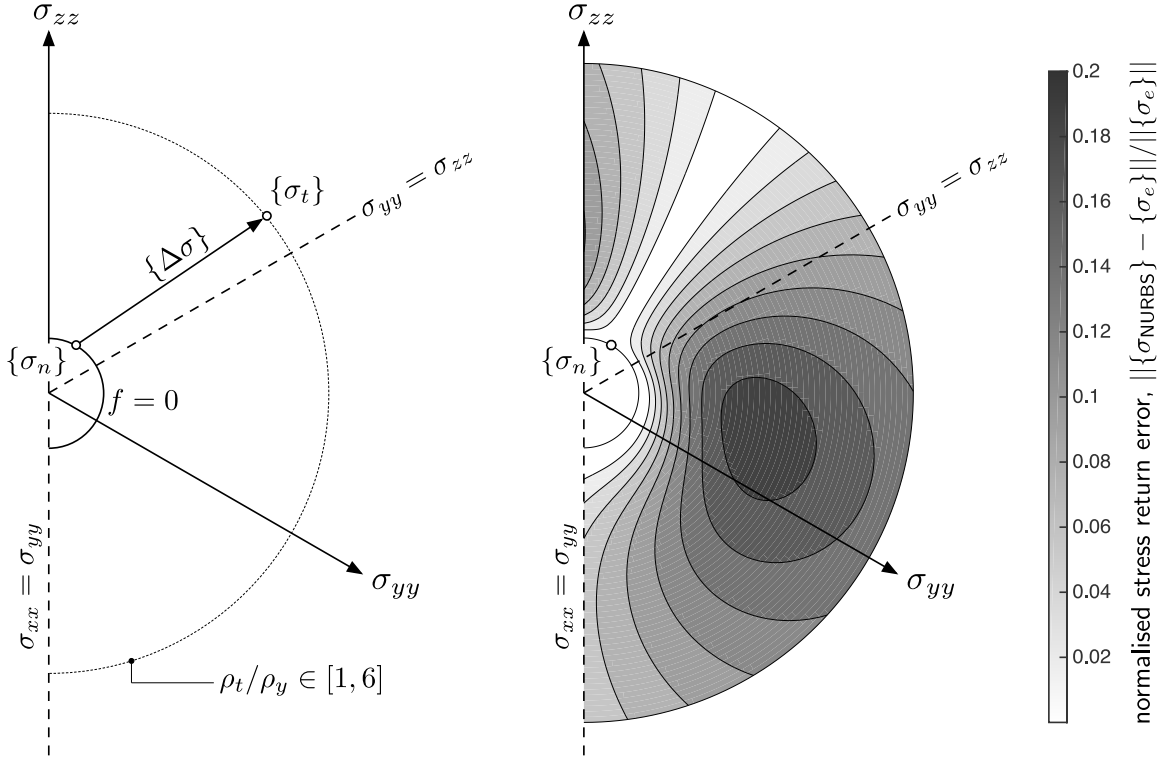


**Figure 1:** Stress return error analysis for an isotropically hardening von Mises NURBS yield envelope.

of 206.9GPa, Poisson's ratio of 0.29 and was modelled using an isotropically hardening von Mises yield surface with associated flow with an initial yield stress of  $\rho_y = 0.45\text{GPa}$ .

Nagtegaal *et al.* [6] provided the small strain analytical limit load for the case of perfect plasticity ( $\alpha = 0$ ), controlled by the stress at the notch  $\sigma_{\text{lim}} \approx 2.97\rho_y$ . The specimen had a total height and width of 30mm and 10mm respectively, with a 2mm unit linking ligament at mid height. For this geometry the small strain perfect plasticity limit load is  $f^{\text{lim}} \approx 2.673\text{kN}$ . Due to symmetry, only one quarter of the specimen was initially discretised using 75 plane strain eight-noded elements with reduced four-point integration, as shown in Figure 3. A displacement of 0.2mm was applied in 20 equal displacement-controlled increments.

Figure 3 shows three different model responses for two finite element discretisations. The three cases are where  $\alpha = 1$  (hardening or expansion of the yield surface, black dashed line),  $\alpha = 0$  (perfect plasticity, fine black line) and  $\alpha = -1$  (softening or contraction of the yield surface, thick grey line). As the mesh is refined the perfect plasticity response approaches the analytical limit load. As expected the hardening and softening responses predict force versus displacement responses above and below the perfect plasticity response, respectively.

The global normalised residual out of balance force

$$\bar{f}_{\text{oobf}} = \frac{\|\{f^{\text{ext}}\} - \{f^{\text{int}}\}\|}{\|\{f^{\text{ext}}\}\|}, \quad (19)$$

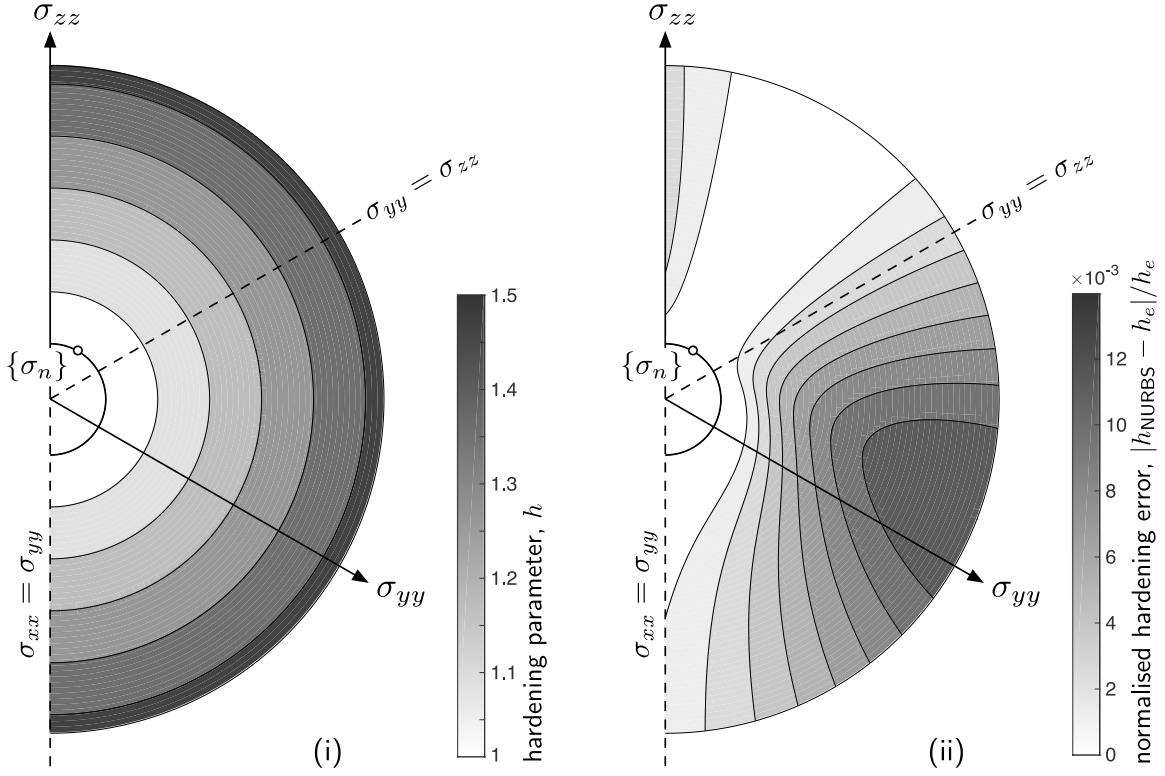


**Figure 2:** (i) stress return hardening parameter values and (ii) errors for an isotropically hardening von Mises NURBS yield envelope.

is given in Table 1 for each of the global Newton iterations for four loadsteps of the 75 element simulation with a softening yield surface with  $\alpha = -1$ . The tolerance on the residual was set to  $1 \times 10^{-8}$ . All of the loadsteps converged in five iterations, or less, with the final iterations within each loadstep approaching a quadratic convergence rate, demonstrating the correct implementation of the algorithmic consistent tangent [10] for the constitutive model, including the case of material softening. For this case by the end of the simulation the minimum size of the yield surface had reduced to 78% of the original.

**Table 1:** Plane strain notched plate convergence for the NURBS implementation of the von Mises yield surface with linear isotropic softening ( $\alpha = -1$ ) with 75 elements ( $1 \times 1\text{mm}$  element size).

NR iteration	loadstep			
	2	3	10	20
1	$8.953 \times 10^{-2}$	$2.502 \times 10^{-1}$	$2.392 \times 10^{-2}$	$1.553 \times 10^{-3}$
2	$6.891 \times 10^{-3}$	$6.605 \times 10^{-2}$	$9.518 \times 10^{-4}$	$8.705 \times 10^{-5}$
3	$4.050 \times 10^{-5}$	$2.205 \times 10^{-3}$	$1.278 \times 10^{-6}$	$8.828 \times 10^{-9}$
4	$1.435 \times 10^{-9}$	$6.933 \times 10^{-6}$	$1.270 \times 10^{-12}$	-
5	-	$6.474 \times 10^{-11}$	-	-

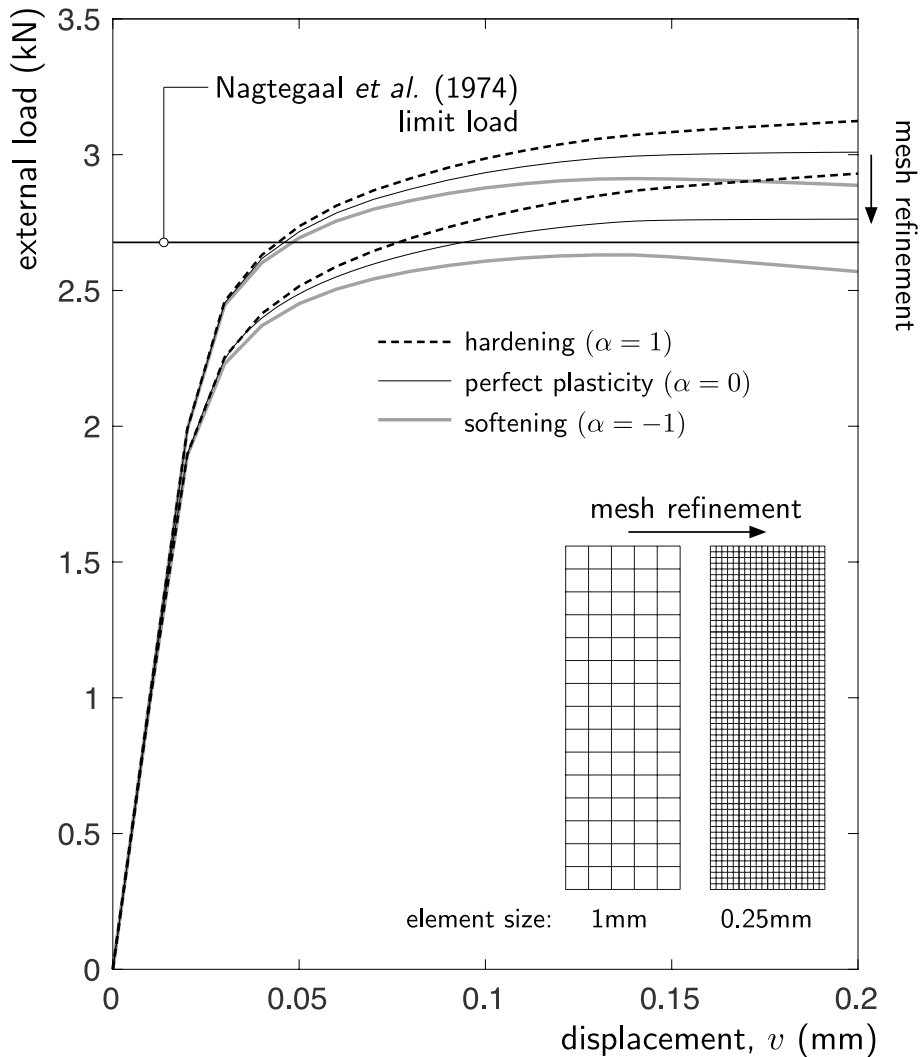


**Figure 3:** Double notched plate with NURBS-based von Mises plasticity with hardening, perfect plasticity and softening responses.

## 5 CONCLUSIONS

This paper extends the NURBS plasticity framework of Coombs et al. [1] to allow: (i) the yield surface to expand (hardening) or contract (softening) under plastic straining and (ii) decoupling the flow direction from the spatial gradient of the surface. This is achieved by allowing the position of the control points to be a function of inelastic straining and for the flow direction to be approximated by a separate NURBS basis. The formulation has been validated at both a material point level and in boundary value simulations.

## References

- [1] W. M. Coombs, O. A. Petit, and Y. Ghaffari Motlagh. NURBS plasticity: Yield surface representation and implicit stress integration for isotropic inelasticity. *Comput. Meth. Appl. Mech. Eng.*, 304:342 – 358, 2016.

- [2] J. A. Cottrell, T. J. R. Hughes, and Y. Bazilevs. *Isogeometric Analysis: Toward Integration of CAD and FEA*. Wiley, New York, 2009.
- [3] R. S. Crouch, H. Askes, and T. Li. Analytical CPP in energy-mapped stress space: application to a modified Drucker-Prager yield surface. *Comput. Methods Appl. Mech. Eng.*, 198(5-8):853–859, 2009.
- [4] E. A. de Souza Neto, D. Perić, M. Dutko, and D. R. J. Owen. Design of simple low order finite elements for large strain analysis of nearly incompressible solids. *Int. J. Solids Struct.*, 33(20-22):3277–3296, 1996.
- [5] A. Kossa and L. Szabó. Exact integration of the von Mises elastoplasticity model with combined linear isotropic-kinematic hardening. *International Journal of Plasticity*, 25(6):1083–1106, 2009.
- [6] J. C. Nagtegaal, D. M. Parks, and J. R. Rice. On numerically accurate finite element solutions in the fully plastic range. *Comput. Meth. Appl. Mech. Eng.*, 4:153–177, 1974.
- [7] L. Piegl and W. Tiller. *The NURBS book*. Springer Science & Business Media, 2012.
- [8] J. C. Simo. Associative coupled thermoplasticity at finite strains: Formulation, numerical analysis and implementation. *Comput. Meth. Appl. Mech. Eng.*, 98(1): 41–104, 1992.
- [9] J. C. Simo and M. S. Rifai. A class of mixed assumed strain methods and the method of incompatible modes. *Int. J. Numer. Meth. Engng.*, 29(8):1595–1638, 1990.
- [10] J. C. Simo and R. L. Taylor. Consistent tangent operators for rate-independent elastoplasticity. *Comput. Meth. Appl. Mech. Eng.*, 48(1):101–118, 1985.
- [11] M. Wilkins. Calculation of elastic-plastic flow. In S. Fernback and M. Rotenberg, editors, *Methods of Computational Physics*, volume 3, 1964.